# Spin glass behavior and colossal negative magnetoresistance of the $p$-$Zn_{1-x}Mn_xTe$ strongly doped with phosphorus

Le Van Khoi,[1,*] W. Dobrowolski,[1] T. Kazimierczuk,[2] A. Rodek,[2] P. Kossacki,[2] R. R. Galazka,[1] and W. Zawadzki[1]

[1]*Institute of Physics, Polish Academy of Sciences, Al. Lotnikow 32/46, 02-668 Warsaw, Poland*

[2]*Institute of Experimental Physics, Faculty of Physics, University of Warsaw, ul. Pasteura 5, 02-093 Warsaw, Poland*

(Received 23 October 2019; revised manuscript received 20 December 2019; accepted 11 February 2020; published 27 February 2020)

Magnetoresistance, ac and dc magnetization, and photoluminescence (PL) experiments have been performed on the $p$-type $Zn_{0.99}Mn_{0.01}Te$ and $Zn_{0.97}Mn_{0.03}Te$ alloys strongly doped with phosphorus (P). The investigated samples exhibit spin glass behavior with ferromagnetic regions near the freezing temperature $T_f = 1.9$ K and colossal negative magnetoresistance (negMR) of $2.2 \times 10^3$ times at 4.2 K for $0 \leqslant B \leqslant \pm 6$ T. The negMR curves contain occurrences of hysteresis providing evidence for the memory effect. Looking for possible ferromagnetic interactions responsible for the spin glass behavior at low hole densities, we observe in PL spectra that the P doping quenches internal recombination in $Mn^{2+}$ ions. This strongly indicates a charge transfer between $Mn^{2+}$ and $P^{2-}$ ions leading to the creation of $Mn^{3+}$ and $P^{3-}$ ions. The creation of $Mn^{3+}$ is confirmed by an observation of strong PL enhancement at excitation energies lower than the band gap and PL study at various temperatures. The resulting simultaneous existence of the mixed valence $Mn^{2+}$ and $Mn^{3+}$ ions can lead to double exchange mechanism of ferromagnetic interaction. Also, $Mn^{3+}$ ions can exhibit a superexchange interaction leading to local ferromagnetic phases.

DOI: 10.1103/PhysRevB.101.054440

## I. INTRODUCTION

Spin glasses, i.e., magnetic systems with randomly competing interactions, have attracted considerable interest in recent decades. A transition to the spin glass (SG) phase in the nonconducting $Zn_{1-x}Mn_xTe$ diluted magnetic semiconductor (DMS) with high Mn density ($0.07 \leqslant x \leqslant 0.70$) was studied some years ago with the use of magnetic susceptibility measurements [1,2]. Similarly to the case of the $Hg_{1-x}Mn_xTe$ and $Cd_{1-x}Mn_xTe$ DMS [3,4], the $Zn_{1-x}Mn_xTe$ alloy is in principle a Heisenberg antiferromagnet in which combined effects of randomness and frustration give rise to spin glass systems at low temperatures. More recently, it was demonstrated that heavy $p$-type doping results in RKKY interactions leading to ferromagnetic (FM) order. This was shown for nitrogen doped $Zn_{1-x}Mn_xTe$ epitaxial layers [5] and $Cd_{1-x}Mn_xTe$ based quantum wells [6,7]. Similarly, doping of bulk $Zn_{1-x}Mn_xTe$ with phosphorus (P) to levels near metal-insulator transition ($\approx 8 \times 10^{24}$ m$^{-3}$) induces the ferromagnetic interaction between $Mn^{2+}$ ions [8,9]. This finding provided a possibility to study the SG transition resulting from the competition between the doping-induced FM interaction and the antiferromagnetic superexchange between the $Mn^{2+}$ ions in low $x$ limit.

The above subject is related to the important and applicable phenomenon of strong negative magnetoresistance (negMR). The standard magnetoresistance, caused by the cyclotron-like trajectories of charge carriers in a magnetic field, is positive and not very large. However, an external magnetic field can influence electrical conductivity in many different ways leading in particular to the negative sign of the effect. Relative size of negMR can amount to many orders of magnitude depending on its origin. So, colossal negMR in $p$-type $Hg_{1-x}Mn_xTe$ was reported and attributed to the spatial growth of the acceptor wave functions with increasing magnetic field [10,11], while colossal negMR in $n$-type $Cd_{1-x}Mn_xSe$ was attributed to the joint effect of the redistribution of electrons between spin subbands and a magnetic polaron [12]. Very large negMR was reported in $(Re)Ni_{1-x}Co_xO_3$ (Re = La, Nd, Sm) and shown to occur when the material underwent the freezing transition to the SG phase [13].

Our work describes the spin glass state in the $p$-type $Zn_{0.99}Mn_{0.01}Te$ and $Zn_{0.97}Mn_{0.03}Te$ strongly doped with phosphorus atoms. We focus on the intermediate hole densities to explore the range between a localized spin glass system and the Zener ferromagnet [14]. In our SG system colossal values of negMR are observed in the vicinity of the freezing temperature. Our considerations are concerned with the competition between antiferromagnetic and ferromagnetic interactions at low hole densities. On the basis of photoluminescence data at various excitation energies and temperatures it is argued that we deal with the double exchange related to the mixed valence $Mn^{2+}$ and $Mn^{3+}$ ions, the latter being created by a charge transfer between $Mn^{2+}$ and $P^{2-}$ ions, or ferromagnetic superexchange interaction between $Mn^{3+}$ ions, or both. The $Mn^{2+}$ to $Mn^{3+}$ charge transfer might also act as a mechanism limiting local density of the hole gas.

The paper is organized as follows. Section II describes sample preparation and experimental methods, Sec. III reports

*lkhoi@ifpan.edu.pl

 

our results on colossal negative magnetoresistance, Sec. IV is concerned with magnetic susceptibility, and Sec. V with photoluminescence. Section VI contains the discussion in which we report the charge transfer and propose mechanisms of ferromagnetic interactions. The paper is concluded by a summary.

## II. SAMPLE PREPARATION AND EXPERIMENTAL METHODS

The P-doped $Zn_{1-x}Mn_xTe$ crystals were grown by the high-pressure Bridgman method from $(ZnTe)_{1-x}(MnTe)_x$ solution in an evacuated ($10^{-6}$ Torr) quartz ampoule coated with pyrolytic graphite. ZnTe and MnTe polycrystal sources were synthesized from 6N purity Zn, Mn, Te elements and weighted to reach desired stoichiometric ratio for a nominal Mn molar content $x_n$. Phosphorus was added in the form of $Zn_3P_2$. The $Zn_{1-x}Mn_xTe$ samples split from the as-grown ingot were additionally subjected to annealing at 1100 K and pressure of 4 MPa of nitrogen gas to improve the composition homogeneity.

The actual Mn content $x$ in each sample was determined by the energy dispersive x-ray fluorescence analysis (EDXFA). The EDXFA measurements were carried out at 300 K using the Spectrace 5000 Tracor Xray spectrometer equipped with Si(Li) detector. The x-ray diffraction (XRD) method with the use of a Siemens D5000 diffractometer was used to determine the lattice constants $a$ of the samples.

For magnetotransport experiments we used six-contact Hall bars with dimensions $5 \times 1 \times 0.2$ mm$^3$ cut from a monocrystal block in a direction perpendicular to the [111] crystal growth axis. Ohmic contacts were fabricated using chemically deposited gold from the $HAuCl_4$ solution. Resistivity and Hall measurements were carried using four-probe method with dc currents between 0.1 and 10 mA. Photoluminescence experiments were performed using two different laser diodes operating at 561 nm (Cobolt Jive561) or 488 nm (Omicron LuxX 488). Oxford superconducting magnet delivered maximum magnetic field of 13 T. Magnetic properties of $Zn_{1-x}Mn_xTe$ were investigated using 7229 LakeShore Susceptometer/Magnetometer allowing us to measure both ac and dc magnetizations.

Figures 1(a) and 1(b) present the measured distribution of Mn content $x$ (open circles) along the ingot length for two $Zn_{1-x}Mn_xTe$ crystals with nominal Mn contents $x_n = 0.05$ and 0.30, respectively. One notes that the actual Mn contents along the middle parts of the ingots are smaller than the nominal (weighted) Mn ones by the factor of about 0.5 and they rapidly increase at the ends of the ingots. This is a clear indication of a segregation of the Mn component during the crystal growth. The variation of the actual Mn content $x(d)$ along the ingot length is described by the classical segregation formula for the directional freezing model [15]

$$x(d) = C_0 k \left(1 - \frac{d}{L}\right)^{k-1}, \qquad (1)$$

where $k$ is the solid/liquid interface segregation coefficient, $C_0$ is the initial Mn concentration in the liquid phase, $d$ is the distance from the bottom of the ingot, $L$ is the total length of the ingot. The solid lines in Figs. 1(a) and 1(b) represent fits of

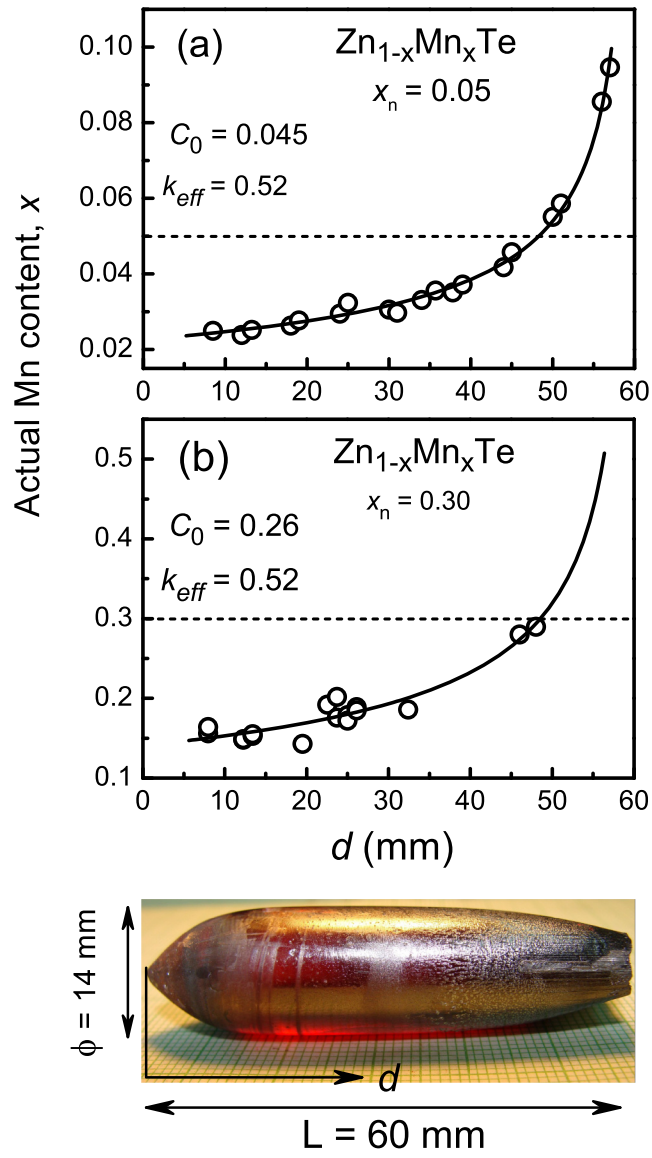


FIG. 1. Actual Mn concentration $x$ in $Zn_{1-x}Mn_xTe$ with nominal concentrations (a) $x_n = 0.05$ and (b) $x_n = 0.30$ as functions of the distance $d$ from the bottom of the ingot along the growth axis. Dashed lines mark the values of $x_n$. Picture of a $Zn_{1-x}Mn_xTe$ monocrystal is also shown.

Eq. (1) to the measured Mn distribution. The best fits gave the values of $k = 0.52$ for both $x = 0.05$ and 0.30. The value of $k$ is smaller than unity indicating that the $Zn_{1-x}Mn_xTe$ crystals grown from the melt are characterized by large Mn concentration variation along the growth axis. On the other hand, this gives us a possibility to obtain samples with different Mn contents produced in the same technological regime.

In order to examine the crystallographic quality of the $Zn_{1-x}Mn_xTe$ crystals we measured the lattice constant $a$ as a function of the Mn concentration $x$ in $Zn_{1-x}Mn_xTe$. Figure 2 presents plot of values of $a$ versus $x$. The solid line is the fit of the Vegard law,

$$a(x) = 6.100 + 0.281x \ \text{(Å)}. \qquad (2)$$

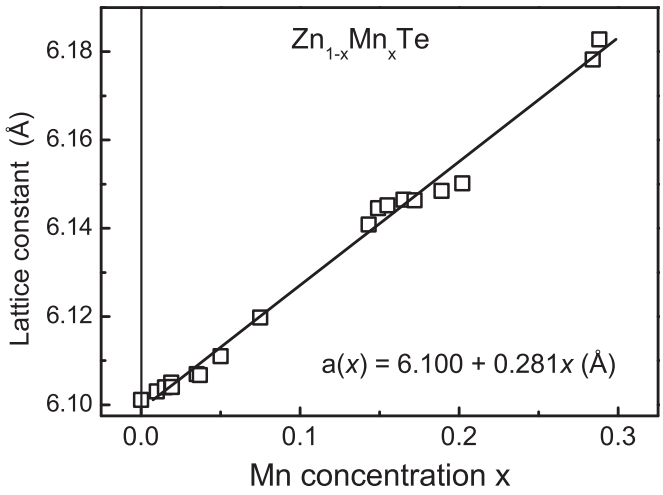


FIG. 2. Variation of the lattice constant $a$ versus Mn concentration in $Zn_{1-x}Mn_xTe$. The solid curve is a linear fit.

Here, $0 \leqslant x \leqslant 0.30$. The linear increase of $a$ with $x$ proves good crystallographic quality of our crystals. The growth of $a$ is in agreement with the fact that the tetrahedral radius of Mn atoms (1.33 Å) is larger than that of Zn atoms (1.225 Å) [16].

For magnetic measurements we used two samples with the actual concentrations $x = 0.008$ and 0.029, and respectively denoted them as S1 and S2. For magnetotransport experiments we used two other samples with the actual Mn contents equal to 0.01 and 0.03.

### III. NEGATIVE MAGNETORESISTANCE

Figure 3 shows low-temperature negative magnetoresistance of $Zn_{0.99}Mn_{0.01}Te$ strongly doped with phosphorus. As the temperature decreases, the zero-field resistance $R_0$ strongly grows: $R_0(1.3\ \text{K})/R_0(4.2\ \text{K}) \approx 10^4$, indicating the increasing localization of holes. In parallel, the negMR amplitude becomes drastically larger. At $T = 1.3$ K, negMR reaches colossal magnitude going from $4.7 \times 10^3\ \Omega$ to $1.2\ \Omega$ as $B$ increases from 0 to $\pm 6$ T. The temperature dependence of resistance (not shown) indicates that the sample is an insulator at low temperatures.

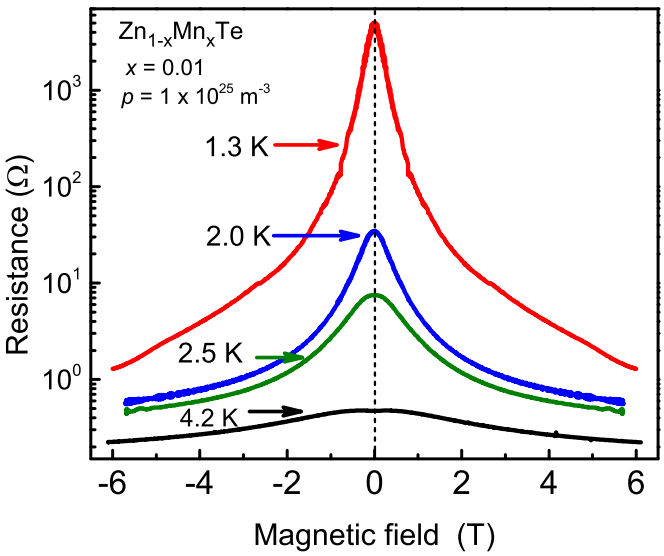


FIG. 3. Low-temperature negative magnetoresistance of $Zn_{0.99}Mn_{0.01}Te$ doped with phosphorus versus magnetic field. At $T = 1.3$ K the negative magnetoresistance reaches colossal magnitude of R(0 T)/R(6 T) $\approx 10^4$.

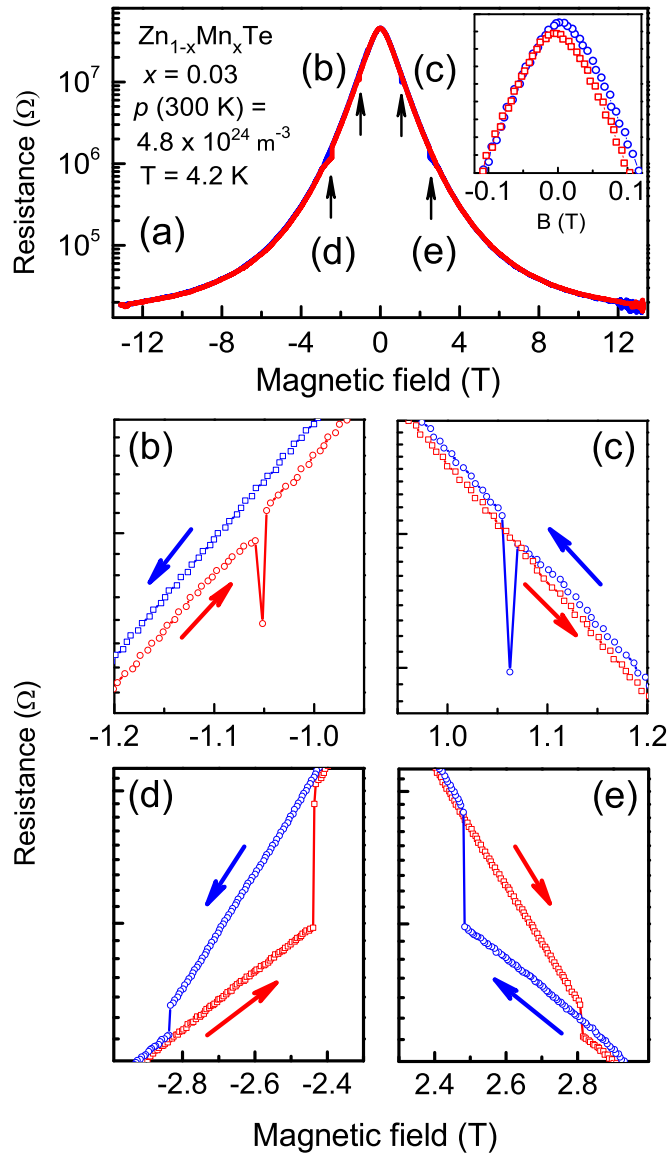


FIG. 4. (a) Colossal negative magnetoresistance of $Zn_{0.97}Mn_{0.03}Te$ doped with phosphorus versus magnetic field. The inset shows asymmetric hysteresis near B = 0. Figures 4(b), 4(c), 4(d), and 4(e) show the details of features in the negMR curve marked by the arrows in Fig. 4(a). The arrows indicate directions of field sweeps evidencing the memory effect, see text. Magnetic field sequence was $-0.6\ \text{T} \rightarrow -13\ \text{T} \rightarrow +13\ \text{T} \rightarrow -0.6\ \text{T}$.

Colossal negMR is also observed on the $Zn_{0.97}Mn_{0.03}Te$ sample, as illustrated in Fig. 4(a). It is seen in the inset that near $B = 0$ there exists an asymmetric hysteresis in the proximity of the zero field, indicating that we deal with ferromagnetic inclusions (similar hysteresis was observed in Ref. [17]). Also, the negMR curve exhibits features (marked

with arrows) shown in more detail in Figs. 4(b), 4(c), 4(d), and 4(e). The symmetric hysteresis is observed which we attribute to the ferromagnetic regions in the sample. The arrows indicate field sweep directions. Larger vertical MR jumps occur on both sides after the sample has been subjected to the maximum field, while the smaller jumps occur after it has passed the zero field giving evidence to the memory effect. The very high resistance near $B = 0$, as well as its temperature dependence (not shown), indicate that also this sample is at low temperatures an insulator with localized holes.

The occurrence of the resistance hysteresis can be understood if we keep in mind that an electric current flowing through dilute magnetic semiconductor placed in an external magnetic field becomes spin polarized (SP) due to the giant Zeeman splitting of the conduction and valence bands. The spin-polarization degree of the current increases with increasing magnetic field. This current probes local ferromagnetic (FM) inclusions in the sample. The coupling between the SP current and local FM inclusions leads to the switching of local orientations of magnetization which in turn gives rise to the jump of the sample resistance.

The anomalies in negMR are also seen in the data shown in Fig. 3 taken at 1.3 K. They are not as rich as those demonstrated in Fig. 4.

## IV. MAGNETIC SUSCEPTIBILITY

We observe that despite the heavy doping with phosphorus the $Zn_{1-x}Mn_xTe$ crystals with $x \geqslant 0.03$, not subjected to post-growth annealing, are strongly compensated and exhibit low hole density of $p \leqslant 10^{23}$ m$^{-3}$. However, the post-growth high pressure annealing effectively removes the compensation resulting in the increase of free hole densities

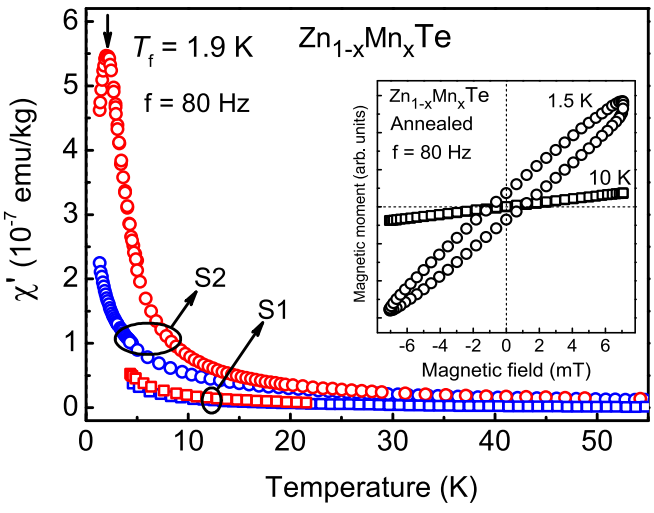


FIG. 5. Real part of ac magnetic susceptibility versus temperature for two $Zn_{1-x}Mn_xTe$ samples before (blue) and after (red) high pressure annealing. The inset shows magnetization values of the annealed sample S2 as functions of magnetic field at two temperatures. At $T > T_f$ the magnetization is linear while at $T < T_f$ one deals with the hysteresis loop.

TABLE I. Parameters of the S1 and S2 samples of $Zn_{1-x}Mn_xTe$:P. Quantities $p_b$ and $p_a$ denote hole densities before and after annealing. The effective (magnetically active) Mn contents $x_{\text{eff}}$ and the Curie-Weiss temperature before $T^b_{CW}$ and after $T^a_{CW}$ annealing were determined from magnetic susceptibility measurements in a temperature range $1 < T < 40$ K.

| Samples | $x_{\text{eff}}$ | $p_b$ (m$^{-3}$) | $p_a$ (m$^{-3}$) | $T^b_{CW}(K)$ | $T^a_{CW}$ (K) |
|---|---|---|---|---|---|
| S1 | 0.008 | $1.2 \times 10^{25}$ | $8.8 \times 10^{24}$ | 1.2 | 1.7 |
| S2 | 0.029 | $4 \times 10^{23}$ | $4.8 \times 10^{24}$ | −2.4 | +2.1 |

up to $p = 4.8 \times 10^{24}$ m$^{-3}$ and magnetic susceptibility of the samples.

Figure 5 presents the real components $\chi'(T)$ of the ac magnetic susceptibility measured at 80 Hz as functions of temperature for two $Zn_{0.992}Mn_{0.008}Te$ (labeled S1) and $Zn_{0.97}Mn_{0.029}Te$ (labeled S2) samples. Parameters of the S1 and S2 samples are presented in Table I. It is seen that the annealing enhances $\chi'(T)$ by a factor of 1.4 and 3 at $T = 4.2$ K for S1 and S2, respectively. The sample S2 exhibits a cusplike peak at $T_f \approx 1.9$ K indicating a transition from paramagnetic to spin-glass phase. We reach this conclusion since the transition occurs rather slowly (over 3 degrees K), see Ref. [18]. The inset shows two magnetization values versus magnetic field, measured for the S2 sample at the temperatures higher and lower than $T_f$. At $T = 10$ K the magnetization is a linear function of the field in both field directions, while at $T = 1.5$ K it exhibits a hysteresis loop. This indicates that at $T \leqslant T_f$ there exist local regions in which the Mn spins are ferromagnetically coupled. The initial increase of $\chi'(T)$ in both annealed samples occurs at about 30 K indicating that the ferromagnetic correlation sets in at temperatures appreciably higher than the freezing temperature. We note that the same annealing procedure applied to undoped samples with $x = 0.01, 0.03, 0.07$ causes no change of $\chi'(T)$ (not shown here). This indicates that the increase of $\chi'(T)$ is connected with the phosphorus doping and the post-growth heat treatment.

In Fig. 6 we show the real component $\chi'(T)$ of the ac magnetic susceptibilities measured for the annealed S2 sample as functions of temperature at three different ac field frequencies. The cusplike peaks at $T_f$ shift to higher temperatures with growing frequency. The inset in Fig. 6 shows a plot of freezing temperature $T_f$ vs field frequency. The relative shift $T_f$ per the order of magnitude of frequency $R = \Delta T_f/[T_f \times \log(f)]$ is equal to 0.082. Since this behavior is well known for typical spin-glass systems [19,20] we conclude that the sample freezes from the paramagnetic to the spin-glass phase. The magnetization loop in the inset of Fig. 5 shows that our sample is not a conventional spin glass but rather a cluster glass (mictomagnet). Recalling that the undoped $Zn_{1-x}Mn_xTe$ for small $x$ is a paramagnet in which the dominating interaction between $Mn^{2+}$ ions is the antiferromagnetic superexchange [21], we infer that the magnetic properties of $Zn_{1-x}Mn_xTe$ described above are related to the doping with phosphorus. We add that also our annealed S2 sample is an insulator at low temperatures. Figure 7 shows plots of the inverse paramagnetic susceptibility versus temperature for S1 and S2 samples before and after annealing. According to the Curie-Weiss law,

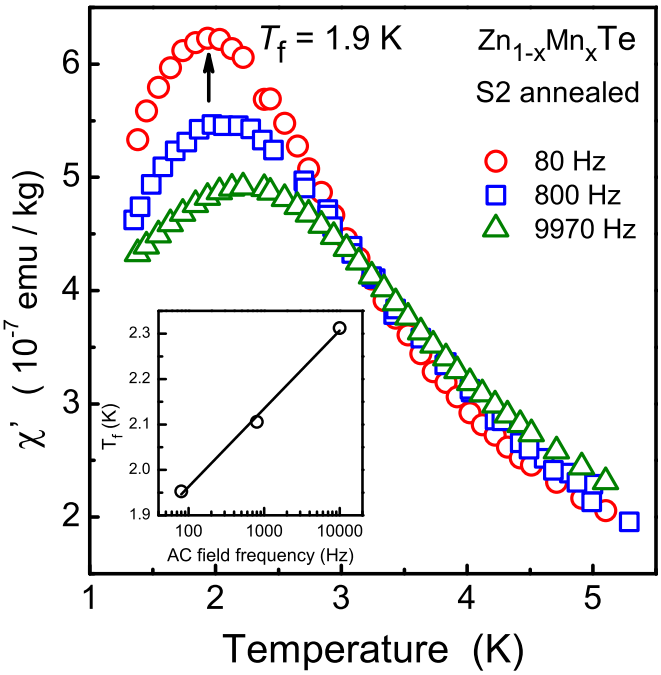


FIG. 6. Real components of the ac magnetic susceptibility $\chi'(T)$ versus temperature at three frequencies for the annealed sample S2 presented in Fig. 5. The observed behavior is typical for the spin glass near freezing temperature $T_f$. Inset shows the shift of $T_f$ with the field frequency.

$1/\chi'(T)$ can be expressed as follows

$$\frac{1}{\chi'} = \frac{T - T_{CW}}{C}, \tag{3}$$

with the Curie constant

$$C = \frac{N_0 x_{\text{eff}} S(S+1) g_{\text{Mn}}^2 \mu_B^2}{3k_B} \tag{4}$$

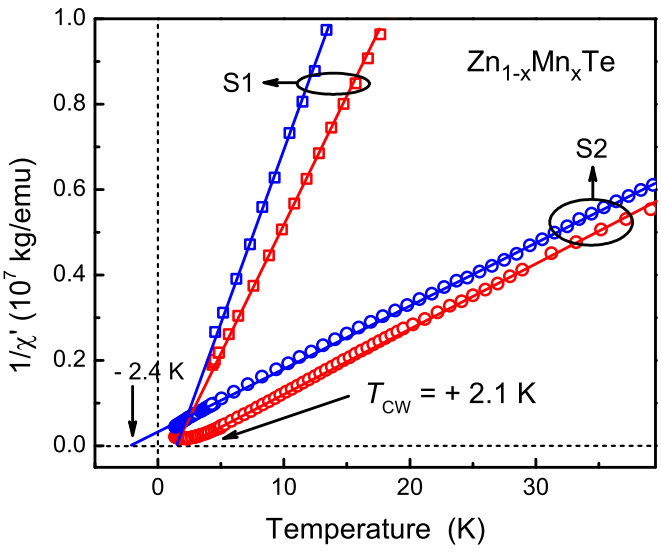


FIG. 7. Inverse ac magnetic susceptibility versus temperature for two S1 and S2 samples before (blue) and after (red) high pressure annealing. The solid lines are linear fits to the data.

where $T_{CW}$ is the paramagnetic Curie-Weiss temperature, the Mn spin is $S = 5/2$; $\mu_B$ is the Bohr magneton; $g_{\text{Mn}} = 2.0$ is the Lande factor. The density of cation sites in ZnTe is $N_0 = 1.76 \times 10^{28}$ m$^{-3}$. The susceptibility $\chi'$ is obtained by subtracting from the experimentally measured susceptibility values $\chi_{\text{exp}}$ diamagnetic susceptibility of the nonmagnetic ZnTe host $\chi_{ZnTe} \approx -2 \times 10^{-7}$ emu/g.

The solid lines in Fig. 7 present linear fits of Eq. (3) to the measured dependences which are used to determine effective Mn content $x_{\text{eff}}$ and the Curie-Weiss temperatures. Our results show a positive shift of $T_{CW}$ caused by the annealing from 1.2 to 1.52 K for S1 and −2.4 K to +2.1 K for S2. Positive signs of $T_{CW}$ indicate the presence of ferromagnetic interactions between Mn ions which dominate the intrinsic antiferromagnetic superexchange in the samples.

We note that despite the fact that hole densities in our S1 and S2 samples are much lower than those of the nitrogen-doped $Zn_{1-x}Mn_xTe$ one with similar Mn content studied in Ref. [5], the values of $T_{CW}$ for S1 and S2 are very close to those reported in Ref. [5]. This comparison indicates that the Mn-Mn FM interaction in our samples must have an origin different from the RKKY mechanism reported in Ref. [5].

## V. PHOTOLUMINESCENCE

Fortunate property of $Zn_{1-x}Mn_xTe$ is that its gap $E_g$ is larger than internal Mn-ion optical transition energies. We show in Fig. 8 photoluminescence spectra of three $Zn_{1-x}Mn_xTe$ samples with $x \approx 0.03$ doped with increasing quantities of P atoms. Figure 8(a) reports the PL spectrum of the undoped sample. The PL maximum at $\hbar\omega = 1.96$ eV is due to internal recombination of $Mn^{2+}$ ions, $^4T_1 \rightarrow {}^6A_1$, as analyzed in Ref. [21]. As one dopes the sample [Fig. 8(b)], the corresponding peak becomes weaker and finally, when the P density is sufficiently high [Fig. 8(c)], the $Mn^{2+}$ peak

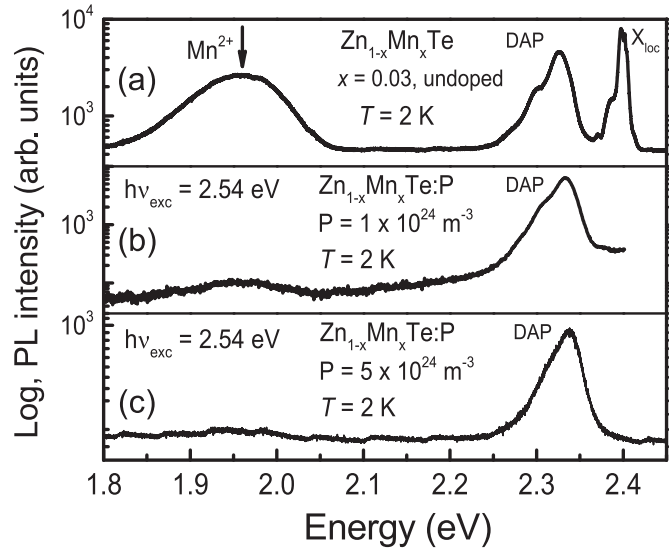


FIG. 8. Photoluminescence spectra of $Zn_{0.97}Mn_{0.03}Te$ doped with phosphorus for three doping levels. The maximum of PL at $\hbar\omega = 1.96$ eV is due to $Mn^{2+}$ ions, see Ref. [21]. As the P doping grows, the $Mn^{2+}$ PL band becomes weaker [Fig. 8(b)] and disappears [Fig. 8(c)].

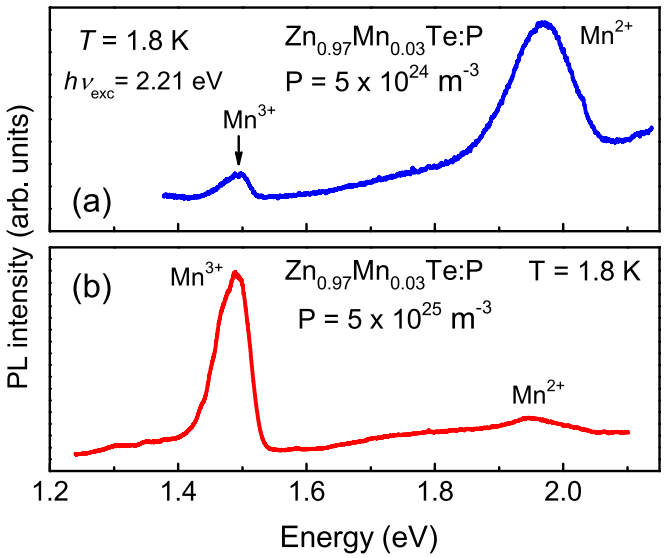


FIG. 9. (a) Photoluminescence spectrum of $Zn_{0.97}Mn_{0.03}Te$ doped with phosphorus for doping density $P = 5 \times 10^{24}$ m$^{-3}$. (b) The same for P doping 10 times stronger. It is seen that the ratio of PL intensities related to $Mn^{2+}$ and $Mn^{3+}$is reversed.

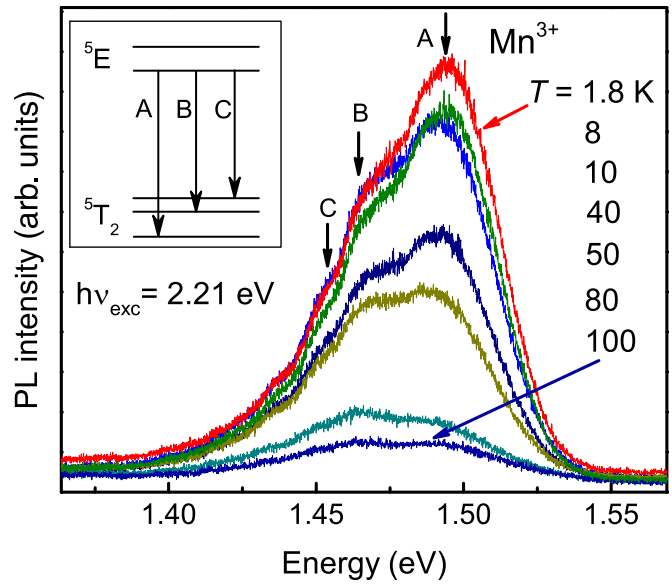


FIG. 10. $Mn^{3+}$ photoluminescence spectra measured on the $Zn_{0.97}Mn_{0.03}Te$ sample presented in Fig. 9(b) at different temperatures. Inset shows the energy level diagram of intra-$Mn^{3+}$ ion transitions corresponding to the A, B, C PL bands.

disappears. An obvious conclusion is that the phosphorus atoms "annihilate" in some sense the $Mn^{2+}$ ions.

In Fig. 9 we present photoluminescence spectra of P-doped $Zn_{0.97}Mn_{0.03}Te$ samples taken with the low energy $\hbar\omega = 2.21$ eV of the exciting laser light. This energy is below that of the gap and donor-acceptor excitations. As seen in Fig. 9(a), for the lower doping the $Mn^{2+}$ PL band is quite strong and the band at 1.49 eV is weak. For stronger doping [Fig. 9(b)] the situation is reversed. This is consistent with our results shown in Fig. 8.

We propose that the PL peak at 1.49 eV in Fig. 9 is due to $Mn^{3+}$ ions. Unlike the intra-$Mn^{2+}$ transitions $^4T_1 \rightarrow {}^6A_1$, the intra-$Mn^{3+}$ transitions $^5E \rightarrow {}^5T_2$ are spin allowed in a cubic crystal field [22]. Therefore, the $Mn^{3+}$ ions can be directly excited by photons with an energy corresponding to the $^5E \rightarrow {}^5T_2$ transition. Figure 10 shows PL spectra of $Mn^{3+}$ ions in the sample presented in Fig. 9(b), excited by laser light with the photon energy 2.21 eV at different temperatures. The spectra consist of three subbands at 1.493 (A), 1.466 (B), and 1.453 (C) eV. Similarly to the intra-$Mn^{2+}$ spectra of Figs. 8 and 9, the shape and spectral position of the $Mn^{3+}$ spectra are independent of the Mn content and temperature. This feature strongly confirms our conjecture concerning the identity of intraionic $Mn^{3+}$ peaks. We consider the identification of $Mn^{3+}$ in the $Zn_{1-x}Mn_xTe$ as one of the important results of our study.

The existence of $Mn^{3+}$ was reported by various authors [23–26]. In particular, Zenneck *et al.* [23] studying photoluminescence from GaN:Mn observed internal $Mn^{3+}$ recombination $^5E \rightarrow {}^5T_2$ at 1.41 eV. Clearly, one cannot expect the same PL energy in our case since we deal with a different material, but the phenomenon of charge transfer discussed below strongly suggests that the lower PL band of 1.49 eV is in fact due to the internal radiative transition $^5E \rightarrow {}^5T_2$ of the $Mn^{3+}$ ions.

## VI. DISCUSSION

Since the RKKY interaction needs a considerable number of holes to produce ferromagnetism in the whole sample, the question arises what is the underlying mechanism for the ferromagnetic interaction seen in our $Zn_{1-x}Mn_xTe$ samples with free hole density smaller than the Mott critical density $N_c = 8 \times 10^{24}$ m$^{-3}$. This problem was raised before [5,27], but until present its satisfactory explanation does not seem to exist. Our results on the spin-glass behavior and the corresponding negMR are similar to those observed by Perez *et al.* [13] on $(RE)Ni_{0.3}Co_{0.7}O_3$ oxides. The authors concluded that a simultaneous presence of Ni and Co was needed to develop competitive ferro- and antiferromagnetic interactions in their compounds. It was suggested that the large electronegativity of $Ni^{3+}$ could induce a charge transfer between the $Ni^{3+}$ and $Co^{3+}$ resulting in the appearance of $Ni^{2+}$ and $Co^{4+}$. Then the ferromagnetic interaction could result from the mixed valence $Co^{3+}$-$Co^{4+}$ interaction by a mechanism similar to the double exchange. Qualitatively, negMR was thought to occur because the size of ferromagnetic domains increases as the magnetic field is applied, resulting in more metallic paths in the sample. The charge transfer in wide gap GaN:(Mn,Mg) was also observed and discussed in Ref. [28].

One can think of an analogous situation in our case. Because the electronegativity of P atoms (equal to 2.19) is stronger than that of Te (2.10) and Mn (1.55) [29], the P doping can result in the charge transfer:

$$Mn^{2+} + P^{2-} \rightarrow Mn^{3+} + P^{3-}$$

leading to the appearance of $Mn^{3+}$ ions and limiting the local hole gas density. A simultaneous presence of $Mn^{2+}$ and $Mn^{3+}$ ions can in turn lead to possible local ferromagnetic double

exchange interaction via the $Te^{2-}$ ions:

$$Mn^{2+}(\uparrow) + Te^{2-}(\uparrow\downarrow) + Mn^{3+}(\uparrow) \Longleftrightarrow Mn^{3+}(\uparrow) + Te^{2-}(\uparrow\downarrow) + Mn^{2+}(\uparrow).$$

Such a possibility was suggested for $La_{1-x}Zr_xMnO_3$ [30]. The charge transfer between $Mn^{2+}$ and $P^{2-}$ ions explains well the quenching of the $Mn^{2+}$ PL band by the P doping seen in Figs. 8(b) and 8(c). Simultaneous existence of $Mn^{2+}$ and $Mn^{3+}$ ions leading to multiphase magnetic ordering was reported for Mn-doped CdSe [31].

The problem with the quantitative explanation in our case is that, in the sample with $x = 0.03$ one has $N_0x = 1.76 \times 10^{28} \times 0.03 = 5.28 \times 10^{26}$ $Mn^{2+}$ ions in $m^{-3}$. On the other hand, with our P doping density we could have roughly $1 \times 10^{24}$ $Mn^{3+}$ ions in $m^{-3}$, i.e., there exist many more $Mn^{2+}$ ions than $Mn^{3+}$ ones in the whole sample. However, it can be seen in Fig. 8 that *locally* one can quench almost all photoluminescence coming from $Mn^{2+}$ ions. This means that *locally* one can have comparable numbers of $Mn^{3+}$ and $Mn^{2+}$ ions which should be enough to achieve a local ferromagnetic phase and lead to the spin glass phase.

Interestingly, there exists another possibility for ferromagnetic interaction. It had been established that in zinc chalcogenides with $Cr^{2+}$ paramagnetic ions the *p-d* interactions are ferromagnetic [32]. The origin of this phenomenon was considered and nearest-neighbor *d-d* superexchange integrals in Cr-based DMS were calculated [33]. It was found that there existed extended energy regions where the calculated superexchange was ferromagnetic. Since $Cr^{2+}$ and $Mn^{3+}$ ions have the same core $3d^4$ shell, one can easily imagine that the superexchange interaction between $Mn^{3+}$ ions also leads to ferromagnetic local regions. We conclude that there are in principle two possible mechanisms of ferromagnetic interactions in our $Zn_{1-x}Mn_xTe$ alloy doped with phosphorus. Finally, we emphasize that there exists a so-called two fluid model in which weakly localized holes can mediate the RKKY interaction [34]. In other words, the weakly bound holes would not participate in the transport but could mediate in the ferromagnetism.

As mentioned above, it appears that our $Zn_{1-x}Mn_xTe$ material is not a typical spin glass at low temperatures. This problem requires further studies, see Refs. [35,36].

## VII. SUMMARY

To summarize, by doping $Zn_{1-x}Mn_xTe$ with phosphorus we can control the charge state of Mn ions. We observed that the *p*-type $Zn_{0.99}Mn_{0.01}Te$ and $Zn_{0.97}Mn_{0.03}Te$ strongly doped with phosphorus exhibit at low temperature insulator conditions spin glass properties and colossal negative magnetoresistance. Looking for the origin of local ferromagnetic regions at small number of holes, photoluminescence experiments were performed indicating that the charge transfer $Mn^{2+} + P^{2-} \rightarrow Mn^{3+} + P^{3-}$ ions occurs producing $Mn^{3+}$ ions. The existence of $Mn^{3+}$ ions is confirmed by photoluminescence experiments. The simultaneous presence of $Mn^{2+}$ and $Mn^{3+}$ gives a possibility of local ferromagnetic double exchange interaction between the mixed-valence ions. The second possible mechanism is a possibility of superexchange interaction between $Mn^{3+}$ ions also leading to ferromagnetic local regions. The conclusive choice among the above mechanisms calls for further investigations.

## ACKNOWLEDGMENT

It is our pleasure to thank Prof. Andrzej Mycielski of the Institute of Physics, Polish Academy of Science for his interest and elucidating discussion.

[1] S. P. McAlister, J. K. Furdyna, and W. Giriat, Phys. Rev. B **29**, 1310 (1984).
[2] A. Twardowski, C. J. M. Denissen, W. J. M. de Jonge, A. T. A. M. de Waele, M. Demianuk, and R. Triboulet, Solid State. Commun. **59**, 199 (1986).
[3] S. Nagata, R. R. Galazka, D. P. Mullin, H. Akbarzadeh, G. D. Khatak, J. K. Furdyna, and P. H. Keesom, Phys. Rev. B **22**, 3331 (1980).
[4] R. R. Galazka, S. Nagata, and P. H. Keesom, Phys. Rev. B **22**, 3344 (1980).
[5] D. Ferrand, J. Cibert, A. Wasiela, C. Bourgognon, S. Tatarenko, G. Fishman, T. Andrearczyk, J. Jaroszyński, S. Koleśnik, T. Dietl, B. Barbara, and D. Dufeu, Phys. Rev. B **63**, 085201 (2001).
[6] A. Haury, A. Wasiela, A. Arnoult, J. Cibert, S. Tatarenko, T. Dietl, and Y. Merle d'Aubigné, Phys. Rev. Lett. **79**, 511 (1997).
[7] H. Boukari, P. Kossacki, M. Bertolini, D. Ferrand, J. Cibert, S. Tatarenko, A. Wasiela, J. A. Gaj, and T. Dietl, Phys. Rev. Lett. **88**, 207204 (2002).
[8] H. Kępa, V. K. Le, C. M. Brown, M. Sawicki, J. K. Furdyna, T. M. Giebultowicz, and T. Dietl, Phys. Rev. Lett. **91**, 087205 (2003).
[9] Le Van Khoi, M. Sawicki, K. Dybko, V. Domuchovski, T. Story, T. Dietl, A. Jędrzejczak, J. Kossut, and R. R. Gałązka, Phys. Status Solidi B **229**, 53 (2002).
[10] T. Wojtowicz and A. Mycielski, Physica B+C **117-118**, 476 (1983).
[11] J. K. Furdyna, J. Appl. Phys. **64**, R29 (1988).
[12] T. Dietl, L. Swierkowski, J. Jaroszynski, M. Sawicki, and T. Wojtowicz, Phys. Scr. **T14**, 29 (1986).
[13] J. Perez, J. Garcia, J. Blasco, and J. Stankiewicz, Phys. Rev. Lett. **80**, 2401 (1998).
[14] T. Dietl, H. Ohno, F. Matsukura, J. Cibert, and D. Ferrand, Science **287**, 1019 (2000).
[15] B. Pamplin, *Crystal Growth* (Pergamon Press, Oxford, 1980).
[16] J. K. Furdyna and J. Kossut, Superlattices Microstruct. **2**, 89 (1986).
[17] T. Mochizuki. R. Masutomi, and T. Okamoto, Phys. Rev. Lett. **101**, 267204 (2008).
[18] W. Dobrowolski, M. Arciszewska, B. Brodowska, V. Domukhovski, V. K. Dugaev, A. Grzęda, I. Kuryliszyn-Kudelska, M. Wójcik, and E. I. Slynko, Sci. Sintering **38**, 109 (2006).
[19] J. L. Tholence, Solid State Commun. **35**, 113 (1980).
[20] J. A. Mydosh, J. Magn. Magn. Mater. **157-158**, 606 (1996).

[21] Le Van Khoi, R. R. Galazka, and W. Zawadzki, Phys. Rev. B **97**, 214435 (2018).
[22] S. Marcet, D. Ferrand, D. Halley, S. Kuroda, H. Mariette, E. Gheeraert, F. J. Teran, M. L. Sadowski, R. M. Galera, and J. Cibert, Phys. Rev. B **74**, 125201 (2006).
[23] J. Zennect, T. Niermann, D. Mai, M. Roever, M. Kocan, J. Malindretos, M. Seibt, A. Rizzi, N. Kaluza, and H. Hardtgen, J. Appl. Phys. **101**, 063504 (2007).
[24] A. Wolos, A. Wysmolek, M. Kaminska, A. Twardowski, M. Bockowski, I. Grzegory, S. Porowski, and M. Potemski, Phys. Rev. B **70**, 245202 (2004).
[25] T. Graf, M. Gjukic, M. S. Brandt, M. Stutzmann, and O. Ambacher, Appl. Phys. Lett. **81**, 5159 (2002).
[26] R. Y. Korotkov, J. M. Gregie, and B. W. Wessels, Appl. Phys. Lett. **80**, 1731 (2002).
[27] M. Sawicki, V. K. Le, L. Hansen, D. Ferrand, L. W. Molenkamp, A. Waag, and T. Dietl, Phys. Status Solidi B **229**, 717 (2002).
[28] T. Devillers, M. Rovezzi, N. Gonzalez Szwacki, S. Dobkowska, W. Stefanowicz, D. Sztenkiel, A. Grois, J. Suffczynski, A. Navarro-Quezada, B. Faina, T. Li, P. Glatzel, F. d'Acapito, R. Jakiela, M. Sawicki, J. A. Majewski, T. Dietl, and A. Bonanni, Sci. Rep. **2**, 722 (2012).
[29] A. L. Allred, J. Inorg. Nucl. Chem. **17**, 215 (1961).
[30] S. Roy and N. Ali, J. Appl. Phys. **89**, 7425 (2001).
[31] O. Halder, B. Satpati, P. Rajput, N. Mohapatra, S. N. Jha, J. Suffczynski, W. Pacuski, and S. Rath, Sci. Rep. **9**, 1804 (2019).
[32] W. Mac, Nguyen The Khoi, A. Twardowski, J. A. Gaj, and M. Demianiuk, Phys. Rev. Lett. **71**, 2327 (1993).
[33] J. Blinowski, P. Kacman, and J. A. Majewski, Phys. Rev. B **53**, 9524 (1996).
[34] M. A. Paalanen and R. N. Bhatt, Physica B **169**, 223 (1991).
[35] B. Barbara, A. P. Malozemoff, and Y. Imry, Phys. Rev. Lett. **47**, 1852 (1981).
[36] B. Barbara, Phys. Rev. Lett. **99**, 177201 (2007).